Analysis of simulation technique for steady shock waves in materials with analytical equations of state

Evan J. Reed,[1,*] Laurence E. Fried,[1] William D. Henshaw,[2] and Craig M. Tarver[1]
[1]*Chemistry and Materials Science Directorate, Lawrence Livermore National Laboratory, Livermore, California 94550, USA*
[2]*Center for Applied Scientific Computing, Lawrence Livermore National Laboratory, Livermore, California 94550, USA*
(Received 1 February 2006; published 20 November 2006)

We calculate and analyze a thermodynamic limit of a multiscale molecular dynamics based scheme that we have developed previously for simulating shock waves. We validate and characterize the performance of the former scheme for several simple cases. Using model equations of state for chemical reactions and kinetics in a gas and a condensed phase explosive, we show that detonation wave profiles computed using the computational scheme are in good agreement with the steady state wave profiles of hydrodynamic direct numerical simulations. We also characterize the stability of the technique when applied to detonation waves and describe a technique for determining the detonation shock speed.

DOI: 10.1103/PhysRevE.74.056706 PACS number(s): 47.11.St, 47.40.Rs, 82.40.Fp

I. INTRODUCTION

Progress in understanding the microscopic details and kinetics of shocked materials has been extremely difficult. The states of matter found behind a shock front and the kinetics of the formation of these states can determine the structure of a steady shock wave. In general, these states and kinetics are determined by the dynamical pathway that the material follows through the shock. When the material behind the shock front is sufficiently close to equilibrium, it is possible to consider the dynamical pathway as a time-dependent thermodynamic trajectory through states with well-defined thermodynamic quantities.

In many cases, shock waves in materials can be reasonably described as rapid jumps in state from the pre-shock state to the post-shock state with transition periods on the order of the Debye period. Examples include waves with purely elastic deformation and shocks at very high temperatures where a thermodynamically stable state is rapidly reached. In other cases, shock waves in materials can be best described by a much slower transition between the pre-shock state and the final shock state. This transition occurs through a sequence of intermediate thermodynamic states and material phases at kinetic rates that are determined by the thermodynamic states and material phases. Examples of such shocks are steady detonation waves in explosives where numerous chemical species form from the beginning of the shock to the end of the shock. The kinetics of the formation of these species determine shock wave profile details. Shocked material in a detonating explosive can take nanoseconds or longer to reach a final reacted state, called the Chapman-Jouguet state. Other examples of this type of wave include plastic deformation waves with slow kinetics and other chemically reactive systems like hydrocarbons [1]. Experimental measurements in such waves can potentially depend on the time scale on which the measurements are made [2,3]. It is the latter type of shock wave that we focus on in this work.

Significant progress in understanding microscopic details and kinetics of shock waves has been made through molecular dynamics simulations. A number of different techniques exist for the molecular dynamics simulation of shock waves. The most common of these schemes is a direct nonequilibrium molecular dynamics (NEMD) approach (see, for example, Ref. [4]). The NEMD method involves creating a shock at one edge of a large computational cell by assigning some atoms at the cell edge a fixed velocity. The shock propagates across the computational cell to the opposite side. While the NEMD approach captures all the dynamics, the simulation time is limited by the time required for the shock to propagate from one side of the computational cell to the other side. The computational work required by NEMD scales at least quadratically in the evolution time because larger systems are needed for longer simulations to prevent the shock wave from reflecting from the edge of the computational cell and propagating back into the cell. When quantum mechanical methods with poor scaling of computational effort with system size are employed, this approach to shock simulations rapidly becomes impossible.

Within the past few years, new types of shock wave simulation techniques have been developed [5–7]. These techniques utilize thermodynamic restraints (nonrigid constraints) on a computational cell that is usually smaller than a NEMD computational cell. Rather than launching a shock across the computational cell, these approaches constrain the computational cell to thermodynamic jump conditions across a shock. In addition to a Hugoniot-based energy restraint, these techniques utilize a constant volume constraint [5], constant particle velocity restraint [6], or constant stress [7] restraint to converge to the final state of the shock wave.

We have developed a related molecular dynamics technique involving a Rayleigh-line thermodynamic restraint [8,9]. In addition to the final state of the shock, this technique aims to go beyond treatment of the shock as a nearly instantaneous change by capturing the intermediate states found in shocks with slow kinetic processes like detonation waves and other chemically reactive systems. This multiscale technique combines atomistic molecular-dynamics simulations with the Euler or Navier-Stokes equations to achieve

*Electronic address: reed23@llnl.gov

long simulation time and length scales. The thermodynamic states of a molecular dynamics simulation cell are constrained to be those of a steady shock wave given by the Euler equations. For clarity in this work, we will refer to this technique as the multiscale shock technique (MSST).

In this work, we derive a closely related, thermodynamic limit version of the MSST that can be utilized in conjunction with simple analytical equations of state instead of molecular dynamics. While not strictly a multiscale method, we will refer to this version as the thermodynamic-MSST (TMSST) for clarity in this work because it is a limiting case of the MSST. TMSST provides a simple testbed to assess the general performance and stability properties of this multiscale approach to shock simulation for a range of material types. We utilize TMSST to compare steady shock wave profiles to the steady shock wave profiles generated using fully hydrodynamic simulations. We also relate the stability of shock waves to the stability of the technique for detonation waves.

II. COMPUTATIONAL SCHEME

A. Review of molecular dynamics scheme

In this section, we present essential details of the MSST in Ref. [8] in preparation for derivation of a thermodynamic limit in Sec. II B. We wish to constrain the thermodynamic states of a molecular dynamics computational cell to the thermodynamic states that exist within a steady shock described by continuum theory. The thermodynamic states of a steady shock in a continuum can be calculated from the Euler equations for compressible flow,

$$\frac{d\rho}{dt} + \rho\frac{\partial u}{\partial x} = 0, \tag{1}$$

$$\frac{du}{dt} + \tilde{v}\frac{\partial p}{\partial x} = 0, \tag{2}$$

$$\frac{d\tilde{e}}{dt} + p\frac{d\tilde{v}}{dt} = 0. \tag{3}$$

Here, ρ is the density, u is the local material velocity, $\tilde{v} = 1/\rho$ is the specific volume, p is the uniaxial stress ($p=-\sigma_{xx}$), $\tilde{e}$ is the energy per unit mass, and complete time derivatives are $\frac{d}{dt} \equiv \frac{\partial}{\partial t} + u\frac{\partial}{\partial x}$. These equations represent the conservation of mass, momentum, and energy, respectively, everywhere in the wave.

We seek solutions of the Euler equations that are steady in the frame of the shock wave moving at speed v_s by making the substitution $x \to x_0 + v_s t$. This substitution, and integration over x, yields a variation of the Hugoniot relations,

$$u - u_0 = (v_s - u_0)\left(1 - \frac{\rho_0}{\rho}\right), \tag{4}$$

$$p - p_0 = (u_0 - v_s)^2\rho_0\left(1 - \frac{\rho_0}{\rho}\right), \tag{5}$$

$$\tilde{e} - \tilde{e}_0 = p_0\left(\frac{1}{\rho_0} - \frac{1}{\rho}\right) + \frac{(u_0 - v_s)^2}{2}\left(1 - \frac{\rho_0}{\rho}\right)^2. \tag{6}$$

Variables with subscripts 0 are the values before the shock wave and we take $u_0=0$, i.e., the material is initially at rest in the laboratory frame. In the terminology commonly used in shock physics, Eq. (5) for the pressure is the Rayleigh line and Eq. (6) for the energy is the shock Hugoniot at constant shock velocity. These equations apply to a time-independent steady state wave moving at speed v_s. We wish to constrain the thermodynamic states of a molecular dynamics simulation to obey these relations.

In Ref. [8], we showed that a molecular dynamics simulation can be constrained to the thermodynamic states of a steady shock by constraining the stress and energy of the molecular dynamics simulation to Eqs. (5) and (6), respectively. This was accomplished by establishing Hamiltonian-based equations of motion for the atoms and the volume degrees of freedom. The total energy of the molecular dynamics system per unit mass (equivalent to the Hamiltonian divided by the total mass of the computational cell $M \equiv \Sigma_i m_i$ where m_i are the atom masses) is

$$\tilde{E} = \tilde{e}(\{\vec{r}_i\},\{\vec{r}_i\}) + \frac{1}{2}Q\dot{\tilde{v}}^2 - \frac{v_s^2}{2}\left(1 - \frac{\tilde{v}}{\tilde{v}_0}\right)^2 + p_0(\tilde{v} - \tilde{v}_0), \tag{7}$$

where dots denote time derivatives, Q is a masslike parameter for the motion of the volume (with units of mass^2/length^4), $\tilde{e}$ is the energy per unit mass $\left[M\tilde{e} \equiv \Sigma_i \frac{1}{2}m_i\dot{\vec{r}}_i^2 + \phi(\{\vec{r}_i\})\right]$, and the $\{\dot{\vec{r}}_i\}$ and $\{\vec{r}_i\}$ are the velocities and positions of the atoms. Equation (7) is a conserved quantity. We utilize the scaled coordinate scheme of Andersen [10,11] to couple the volume to the atomic positions,

$$\vec{r}_i \equiv A\vec{s}_i, \tag{8}$$

$$\dot{\vec{r}}_i \equiv A\dot{\vec{s}}_i, \tag{9}$$

where $\vec{s}$ is the scaled position (ranging from 0 to 1) of the atom within the computation cell and A is a matrix containing the computational cell lattice vectors in columns. Computational cell volume per mass is $\tilde{v} = \det(A)/M$. The volume equation of motion was shown to be

$$\frac{\ddot{\tilde{v}}}{\tilde{v}_0} = \frac{1}{Q}\frac{\left(-\frac{\partial\tilde{e}}{\partial\tilde{v}}(\{\dot{\vec{r}}_i\},\{\vec{r}_i\}) - p_0\right)}{\tilde{v}_0} - \frac{v_s^2}{Q\tilde{v}_0^2}\left(1 - \frac{\tilde{v}}{\tilde{v}_0}\right). \tag{10}$$

Note that $\frac{\partial\tilde{e}(\{A\dot{\vec{s}}_i\},\{A\vec{s}_i\})}{\partial\tilde{v}} = \frac{\partial\tilde{e}(\{\dot{\vec{s}}_i\},\{\vec{s}_i\},\tilde{v})}{\partial\tilde{v}}$ since only uniaxial strain on A in a fixed direction is allowed; therefore A has one degree of freedom which we choose to denote by $\tilde{v}$.

The equation of motion of the atoms (specialized to the case of an orthorhombic computational cell) is calculated from the Hamiltonian based on Eq. (7),

$$A\ddot{\vec{s}}_i = -\frac{1}{m_i}\frac{\partial\phi}{\partial\vec{r}_i} - 2\dot{A}\dot{\vec{s}}_i, \tag{11}$$

where $-\frac{\partial\phi}{\partial\vec{r}_i}$ is the force on atom i due to the interaction potential ϕ.

B. Thermodynamic limit of the molecular dynamics scheme

In this section, we calculate a thermodynamic limit of the scheme presented in the previous section by replacing the microscopic variables with thermodynamic variables. This thermodynamic limit variant, TMSST, will be used in subsequent sections to demonstrate properties of this multiscale approach to steady shock simulation.

If the molecular dynamics system is in thermodynamic equilibrium, the pressure can be written

$$\frac{\partial \tilde{e}(\{\dot{\vec{s}}_i\},\{\vec{s}_i\},\tilde{v})}{\partial \tilde{v}} \to \frac{d\tilde{e}(T,\tilde{v},\{\lambda_j\})}{d\tilde{v}} \tag{12}$$

$$= \left.\frac{\partial \tilde{e}}{\partial \tilde{v}}\right|_{T,\{\lambda_j\}} + \left.\frac{\partial \tilde{e}}{\partial T}\right|_{\tilde{v},\{\lambda_j\}} \frac{dT}{d\tilde{v}} + \sum_j \left.\frac{\partial \tilde{e}}{\partial \lambda_j}\right|_{\tilde{v},T,\{\lambda_{i\neq j}\}} \frac{d\lambda_j}{d\tilde{v}} \tag{13}$$

$$= -p(T,\tilde{v},\{\lambda_j\}) \tag{14}$$

in the (fluctuationless) infinite particle number limit where the $\{\lambda_j\}$ are additional thermodynamic variables, e.g., reaction parameters for chemical reactions or phase transitions. Equation (10) becomes,

$$\frac{\ddot{\tilde{v}}}{\tilde{v}_0} = \frac{1}{Q}\frac{p(T,\tilde{v},\{\lambda_j\}) - p_0}{\tilde{v}_0} - \frac{v_s^2}{Q\tilde{v}_0^2}\left(1 - \frac{\tilde{v}}{\tilde{v}_0}\right). \tag{15}$$

The Rayleigh condition Eq. (5) can be recovered from Eq. (15) in the case $\ddot{\tilde{v}} \to 0$ and $\dot{\tilde{v}} \to 0$. The volume exhibits stable, damped oscillations about the Rayleigh line. The Hugoniot energy condition Eq. (6) can be recovered from Eq. (15) by substituting $\frac{d\tilde{e}}{d\tilde{v}} = \dot{\tilde{e}}/\dot{\tilde{v}}$ and integrating over time. Therefore Eq. (15) satisfies both constraint Eqs. (5) and (6) when thermodynamic equilibrium exists and $\ddot{\tilde{v}} \to 0$ and $\dot{\tilde{v}} \to 0$. In these cases, the volume and energy track the Rayleigh line and Hugoniot energy condition as the thermodynamic state changes and the thermodynamic trajectory is not significantly influenced by the choice of empirical parameter Q.

Equations of motion for T and $\{\lambda_j\}$ must also be provided. For the molecular dynamics scheme, an equation of motion for the temperature can be directly calculated from the kinetic energy of the atoms,

$$k_B\dot{T} = \frac{d}{dt}\left(\frac{2}{3}\frac{1}{N}\sum_i \frac{1}{2}m_i\dot{\vec{r}}^2\right) \tag{16}$$

$$= \frac{2}{3}\frac{1}{N}\sum_i m_i A\dot{\vec{s}}_i \cdot (\dot{A}\dot{\vec{s}}_i + A\ddot{\vec{s}}_i) \tag{17}$$

$$= -\frac{2}{3}\frac{\dot{\tilde{v}}}{\tilde{v}}k_BT - \frac{2}{3N}\sum_i \dot{\vec{r}}_i \cdot \frac{\partial \phi}{\partial \vec{r}_i}, \tag{18}$$

where we have used the equation of motion for the atoms, Eq. (11). Assuming thermodynamic equilibrium is established and taking the infinite particle limit where $\dot{T} = \dot{T}(\tilde{v},\{\lambda_j\},\dot{\tilde{v}},\{\dot{\lambda}_j\})$, we replace the second term on the right side of Eq. (18) with thermodynamic terms,

$$\frac{\dot{T}}{T_0} = -\Gamma\frac{T}{T_0}\left(\frac{\dot{\tilde{v}}}{\tilde{v}}\right) + \frac{\mu'\dot{\tilde{v}}^2}{\tilde{c}_v T_0 \tilde{v}} + \frac{\tilde{q}\dot{\lambda}}{\tilde{c}_v T_0}. \tag{19}$$

Here, Γ is a Gruneisen parameter which is equal to $\frac{2}{3}$ for an ideal atom gas [i.e., the first term on the right side of Eq. (18)], μ' is a material viscosity parameter ($\mu' = \lambda' + \frac{4}{3}\mu$ where μ and λ' are the first and second viscosity coefficients, respectively, of the Navier-Stokes equations [12]), and we have assumed there is a single chemical reaction $0 \le \lambda \le 1$ that releases energy per unit mass $\tilde{q}$ (see, e.g., Ref. [13]). The heat capacity at constant volume per unit mass is $\tilde{c}_v$. The motivation for the particular form of the viscous term is provided in the next paragraph. Equation (19) represents a specialization of the equations of motion to a particular material system.

For the simple case of $\tilde{e} = \tilde{c}_v T$ and $\tilde{q} = 0$, the pressure calculated using Eq. (19) is $p = -\frac{d\tilde{e}}{d\tilde{v}} = -\frac{\dot{\tilde{e}}}{\dot{\tilde{v}}} = \Gamma\tilde{c}_v\frac{T}{\tilde{v}} - \mu'\frac{\dot{\tilde{v}}}{\tilde{v}}$ where $\Gamma\tilde{c}_v\frac{T}{\tilde{v}}$ is the thermodynamic component and $\mu'\frac{\dot{\tilde{v}}}{\tilde{v}}$ is a viscous component. While the pressure calculated in a molecular-dynamics simulation contains a viscous component, the pressure in continuum scale modeling is usually considered to be the thermodynamic component only. The viscous component in continuum modeling is usually introduced explicitly in the equations of motion through the substitution $p \to p_T - \mu'\frac{\partial u}{\partial x}$ in Eqs. (2) and (3) to obtain the Navier-Stokes equations with no thermal diffusion. In this case, Eqs. (4) and (6) remain unchanged and the Rayleigh line condition for a material element flowing through the shock wave, Eq. (5) becomes

$$p_T - \frac{\mu'}{\tilde{v}}\dot{\tilde{v}} - p_0 = (u_0 - v_s)^2\rho_0\left(1 - \frac{\rho_0}{\rho}\right), \tag{20}$$

where p_T is the thermodynamic pressure. The viscous pressure $-\mu'\frac{\partial u}{\partial x}$ has been evaluated in the moving reference frame of the material where $\frac{\partial}{\partial x} = -\frac{1}{v_s - u}\frac{\partial}{\partial t}$. Therefore the form of the viscous term in Eq. (19) is identical to that of the viscous terms in the Navier-Stokes equations. This term accounts for the irreversible production of heat upon shock compression. While the stress in the molecular dynamics simulations contains some viscous component, this can be supplemented with explicit, Navier-Stokes-type viscosity where the viscous parameter μ' is empirically chosen.

For the equation of motion for λ, we take an Arrhenius rate law,

$$\dot{\lambda} = \sigma \exp\left(\frac{-\epsilon_a}{k_BT}\right)(1 - \lambda). \tag{21}$$

Equations (15), (19), and (21) integrated together along with an equation of state for $\tilde{e}(T,\tilde{v},\lambda)$ provide the time dependence of the thermodynamic variables. At each time step Δt, the basic form of the Verlet algorithm [14,15] can be used to integrate Eq. (15) followed by integration of Eq. (19) using the expression $T(t+\Delta t) = T(t-\Delta t) + 2\dot{T}(t)\Delta t$ and the analogous expression to integrate Eq. (21) with $0 \le \lambda \le 1$. In our

experience, integration of these equations occurs sufficiently fast that a higher order algorithm is unnecessary.

Once the time dependence of $T(t)$ and $\tilde{v}(t)$ have been computed, the particle speed $u(t)$ can be computed using Eq. (4). Spatial profiles of waves can be computed with

$$x(t) = -\int_0^t [\mathrm{v_s} - u(t')]dt'. \tag{22}$$

We note that in the case where the viscous portion of the stress is explicitly defined, the empirical parameter Q can be eliminated by considering the limit $Q \to 0$. In this overdamped limit, the volume equation of motion reduces to

$$\mu' \dot{\tilde{v}} = \tilde{v}\left[p_\mathrm{T} - p_0 - \frac{\mathrm{v_s^2}}{\tilde{v}_0}\left(1 - \frac{\tilde{v}}{\tilde{v}_0}\right)\right]. \tag{23}$$

In this case, the shock solution can be computed using no empirical parameters. However, in this work, we solve Eq. (10) with nonzero Q in the spirit of the molecular dynamics simulations since the viscous component of the stress in the molecular dynamics case cannot be explicitly expressed. In this work, we choose Q sufficiently small to be in the overdamped limit of Eq. (10) where the solution is independent of the precise value of Q and is given by Eq. (23).

C. Stability of simulated waves

The technique presented in the previous section is designed to simulate steady solutions. It is possible to also show that these solutions obey the mechanical stability conditions of a shock wave. This section shows that the constraint technique takes the system through states that satisfy these stability conditions.

There are two criteria for the mechanical stability of a shock wave [16]. The first criterion requires $\mathrm{v_s} > c_0$, where c_0 is the speed of sound in the pre-shock material. The second criterion requires $c_1 + u_1 > \mathrm{v_s}$, where the subscript 1 denotes the post-shock state. The condition that $\mathrm{v_s} < c_0$ can be physically motivated by considering the propagation of sound waves in front of the shock. If $\mathrm{v_s} < c_0$, then pressure waves from behind the shock front can propagate out in front, resulting in an increase of the shock front width and eventual decay of the shock front. Behind the shock, if $c_1 + u_1 < \mathrm{v_s}$ the shock front propagates faster than the speed of sound waves behind it. Compressive energy (in the form of a piston driving the shock, etc.) behind the shock cannot reach the shock front, resulting in a decay of the shock pressure and eventual dissipation.

The equation of motion for the volume Eq. (10) can be shown to constrain the system to thermodynamic states that satisfy the conditions for mechanical shock stability. As an example, consider a shock from state A to state B of Fig. 1. Figure 1 shows Rayleigh lines on a schematic shock Hugoniot for a reactive system with a single reaction parameter λ. First consider only the unreacted $\lambda = 0$ Hugoniot. Equation (10) indicates that volume increases or decreases depending on the relation between the stress (approximately given by the Hugoniot line in Fig. 1) and that of the Rayleigh line stress (given by the straight lines in Fig. 1). When the simulation begins at state A, shock compression will occur if the Rayleigh line is above the Hugoniot in pressure-volume space and the volume is initially slightly on the compressed side of the volume of state A. The slope of the Rayleigh line is $-\mathrm{v_s^2}/\tilde{v}_0^2$. The Hugoniot and isentrope have a first-order tangent at point A [16], providing a Hugoniot slope of $-c_0^2/\tilde{v}_0^2$ at state A. Therefore the stability condition $\mathrm{v_s} > c_0$ must be satisfied at point A if compression proceeds up along the Rayleigh line since the slopes obey the condition $-\mathrm{v_s^2}/\tilde{v}_0^2 < -c_0^2/\tilde{v}_0^2$ which implies $\mathrm{v_s} > c_0$. If the shock speed is chosen such that $\mathrm{v_s} < c_0$, then point A is a stable point of Eq. (10) and no compression will occur.

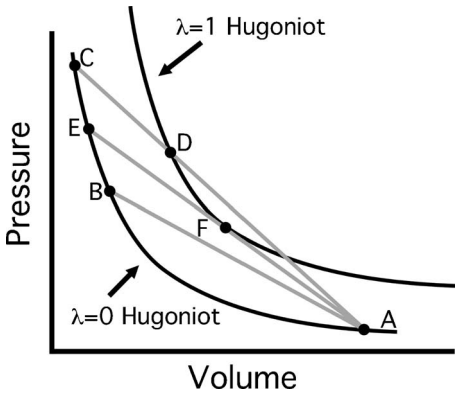

FIG. 1. Rayleigh lines on a Hugoniot for a chemically reactive system with reaction parameter λ. The $\lambda = 0$ Hugoniot represents the unreacted material and the $\lambda = 1$ Hugoniot is fully reacted. The straight Rayleigh lines describe the p-V space thermodynamic pathway of a steady shock.

The volume equation of motion Eq. (10) has stable points (where compression stops) at states where the Rayleigh line intersects the Hugoniot and the Rayleigh line slope magnitude is less than the Hugoniot slope magnitude. Point B in Fig. 1 is an example of such a state. It can be shown that this condition on the Rayleigh line and Hugoniot slopes requires $u_1 + c_1 > \mathrm{v_s}$ which is the stability condition behind the shock front [16]. Therefore Eq. (10) has stable points only where the shock wave mechanical stability conditions are met.

Prior knowledge of the sound speeds is not required when beginning a simulation. If compression occurs at state A, then the stability condition there is satisfied. If compression stops at state B, then the stability condition there is satisfied. A Hugoniot-based constraint technique that follows any other thermodynamic pathway (e.g., constant volume, particle velocity, or stress) does not provide solutions with this property which prevents unphysical thermodynamic conditions in materials where split shocks can form [8]. Note that as a consequence of the instability at point A of Eq. (10), runaway expansion on the tensile strain side of state A is a possible solution. Such an expansion solution may have physical significance if there exists a larger volume where Eq. (10) has a stable solution. Such solutions are expansion shocks and have been predicted to be observable in materials where the Hugoniot has the property that $\frac{\partial^2 p}{\partial v^2}\big|_S < 0$ in some region [12]. However, we focus on the compressive shock solutions. To allow only compressive shock solutions, we begin the simulation with the volume slightly compressed

past point A [we use $V_{start}=(1-10^{-3})V_0$ to bias the simulation to proceed along the compressive branch of the Rayleigh line rather than the expansive branch].

Now consider the case when a single chemical reaction occurs, characterized by the reaction parameter $0 \geq \lambda \geq 1$. As the reaction occurs, λ changes continuously from 0 to 1 forming a family of Hugoniots, of which the $\lambda=0$ and $\lambda=1$ Hugoniots are shown in Fig. 1. Chemical reactions or phase transformations often occur on time scales much slower than the time scale of initial shock compression at the leading edge which molecular-dynamics simulations have shown to be as short as the 100-fs time scale [17,18]. In these cases, the thermodynamic state of the system rapidly advances from state A to state C, for example, and subsequently follows the Rayleigh line down in pressure to state D as the chemical reaction occurs. This scenario represents an overdriven detonation wave. If this reaction occurs on a time scale much longer than the initial compression time scale, the constraint equations will constrain the thermodynamic state of the system to the intersection of the Rayleigh line and the instantaneous, partially reacted Hugoniot at all times.

A particular Rayleigh line is tangent to the $\lambda=1$ shock Hugoniot, as in the case of a shock from state A to state E to state F. In this case, the final state of the shock (state F) has the property that $u_1+c_1=v_s$, a condition of instability. This is commonly referred to as the Chapman-Jouguet state or the sonic plane of the shock. Within the detonation model of Zeldovich, Von Neumann, and Doering, this solution represents the detonation velocity [13]. Rayleigh lines associated with shock speeds smaller than this critical value (like the one from state A to state B) do not intersect the Hugoniot for λ larger than some value. In this case there are no steady solutions that satisfy the shock mechanical stability criteria and the volume equation of motion Eq. (10) will force the volume to grow without bound. Therefore the detonation shock speed can be determined using this technique by performing a series of simulations at various shock speeds. Simulations with well-behaved volume trajectories are above the detonation speed and simulations where the volume blows up to infinity are unphysical (because there is no steady shock solution) and performed at a shock speed less than the detonation speed.

III. APPLICATIONS

A. Ideal gas detonation

In this section, we apply the technique to the calculation of a detonation profile for an ideal gas with a single, energy releasing reaction. We utilize the equation of state

$$\tilde{e} = \tilde{c}_v T - \tilde{q}\lambda, \tag{24}$$

$$p = -\frac{\dot{\tilde{e}}}{\dot{\tilde{v}}} = \Gamma \tilde{c}_v \frac{T}{\tilde{v}} - \mu' \frac{\dot{\tilde{v}}}{\tilde{v}}, \tag{25}$$

where $\Gamma=0.2$, $\tilde{q}=50p_0\tilde{v}_0$ is the energy released by a single chemical reaction with order parameter $0 \leq \lambda \leq 1$. The reaction rate obeys an Arrhenius rate law, Eq. (21), with activation energy barrier $\epsilon_a=3.33k_BT_0$ and $\sigma=5.8\times10^9$ s^{-1} is the kinetic pre-factor for the reaction. We take $T_0=300$ K, $p_0=10^5$ Pa, and $\tilde{v}_0=0.890$ m^3/kg. The viscosity $\mu'=3\times10^{-6}$ kg/ms and $\tilde{c}_v=n_0k_B/(\rho_0\Gamma)=5n_0k_B/\rho_0$ for this ideal gas (n_0 is the initial number density).

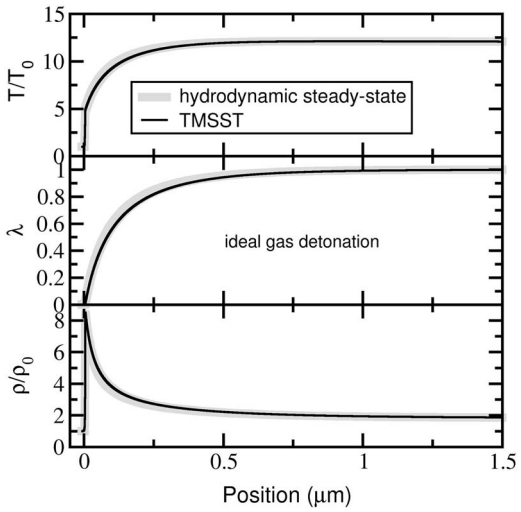

FIG. 2. Comparison of ideal gas detonation wave profiles calculated using the TMSST technique and the steady state of hydrodynamic direct numerical simulations. Excellent agreement is achieved behind the shock front.

Figure 2 shows a profile computed for a detonation wave using the TMSST technique at shock speed $v_s=6.22c_0=2033.71$ m/s. This shock speed is the Zeldovich, Von Neumann, and Doering model detonation speed [13]. The parameter Q in Eq. (10) was chosen to be 8×10^{-20} kg^2/m^4 which provides the overdamped solution, i.e., the parameter Q has no effect on the computed solution. Choosing a larger value of Q results in volume oscillations that decay with time to the overdamped solution. During the first 10 ps of the start of the simulation, rapid compression occurs with little chemical reaction. From this point on, the thermodynamic state changes on a much slower time scale associated with the chemical reaction rate.

Figure 2 compares wave profiles computed with the TMSST to the steady-state profile computed using a hydrodynamic direct numerical solution of the Euler equations for the same final particle velocity u_1. Agreement between the two techniques is excellent. The hydrodynamic direct simulations were performed using the OVERBLOWN adaptive numerical scheme for reactive flow on overlapping grids [19,20]. Simulations started with a detonation wave profile that approximates the expected steady state profile and allowed us to propagate until a steady state was reached. Spatial profiles were computing using Eq. (22).

The OVERBLOWN software solves the Euler equations using a Godunov finite difference scheme containing some artificial viscosity introduced by the integration scheme. The viscosity approximates the second order viscosity term of the Navier-Stokes equations [21]. The amount of viscosity is determined by the grid spacing. The initial rise time of the shock wave (at the start of the chemical reaction, 0 μm in Fig. 2) is determined by the degree of viscosity. The viscos-

ity in the direct hydrodynamic simulations is similar to the viscosity in the TMSST simulations because we have chosen the grid spacing in the hydrodynamic simulations to provide an initial shock rise time similar to that observed in the TMSST simulations. We find that viscosity plays little or no role in the wave profile after the initial shock rise.

We find that the TMSST can be used to compute detonation wave profiles for large activation energies (e.g., $\epsilon_a = 50 k_B T_0$) as easily as for smaller activation energies. However, we find that increasing the activation energy beyond about $\epsilon_a = 3.33 k_B T_0$ (with fixed $\tilde{q}$) can result in unsteady wave propagation in the hydrodynamic direct simulations. This behavior is characterized by oscillatory or chaotic fluctuations in wave profiles and a lack of a moving reference frame in which the detonation wave is steady. Unsteady behavior in one-dimensional (1D) weakly overdriven detonations in high activation energy gaseous mixtures is well known and has been connected to the formation of a cellular detonation structure in higher dimensional simulations (see, e.g., Ref. [22] and references therein). While the solutions computed using the TMSST obey the Euler equations for steady waves, they are not necessarily stable with respect to perturbations in the wave profile. The TMSST provides no information about the stability of computed wave profile with respect to profile perturbations.

B. Condensed phase detonation

In this section, we consider a detonation propagating through a model condensed phase explosive, like HMX or RDX, given by the equation of state

$$\tilde{e} = \tilde{c}_v T + \frac{\alpha}{2}\frac{(\tilde{v}-\tilde{v}_0)^2}{\tilde{v}_0} + \frac{\beta}{3}\frac{(\tilde{v}-\tilde{v}_0)^3}{\tilde{v}_0^2} - \tilde{q}\lambda, \tag{26}$$

$$p = \alpha\frac{(\tilde{v}-\tilde{v}_0)}{\tilde{v}_0} + \beta\frac{(\tilde{v}-\tilde{v}_0)^2}{\tilde{v}_0^2} + \frac{\Gamma\tilde{c}_v T}{\tilde{v}} - \mu'\frac{\dot{\tilde{v}}}{\tilde{v}}. \tag{27}$$

This equation of state [including Eqs. (19) and (21)] has a Mie-Gruneisen form. Mie-Gruneisen equations of state have been used to model high-temperature solids, where the temperature exceeds the Debye temperature [23]. We choose $\alpha = -95$ GPa, $\beta = 52.5$ GPa, $\Gamma = 0.5$, $\tilde{c}_v = 1.5585$ J/g/K, $\tilde{q} = 4$ kJ/g, $\epsilon_a = 8.3415 k_B T_0$, and $\sigma = 9 \times 10^9$ s^{-1}. For the initial state of the simulation, we take $T_0 = 300$ K, $\tilde{v}_0 = 10^{-3}$ m^3/kg. The viscosity parameter is $\mu = 0.3$ kg/ms and the shock speed is $v_s = 11$ km/s.

The parameter Q in Eq. (10) was chosen to be 6×10^{-12} kg^2/m^4 which provides the overdamped solution, i.e., the parameter Q has no effect on the computed solution. Choosing a larger value of Q results in volume oscillations that decay with time to the overdamped solution. As in the ideal gas case, the grid spacing of the hydrodynamic direct simulations was chosen to provide a viscosity that produces a shock front rise distance similar to the TMSST simulations.

Figure 3 compares detonation wave profiles to the steady state profile computed using hydrodynamic direct numerical solutions for the same final particle velocity u_1. Agreement between the two techniques is good. As in the ideal gas case, we expect agreement to be best for the region behind the shock front where the relatively slow chemical reaction occurs and viscosity plays little role.

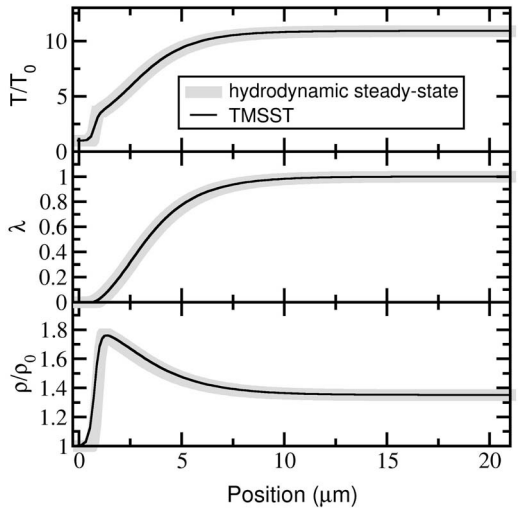

FIG. 3. Comparison of model condensed phase explosive detonation wave profiles calculated using the TMSST technique and the steady state of hydrodynamic direct simulations. Excellent agreement is achieved behind the shock front.

Figure 4 shows a comparison of the thermodynamic pressure-volume space trajectory of the steady state wave of direct hydrodynamic simulations to the TMSST technique. Plotted is the thermodynamic pressure only, with no viscous component. The simulation begins at $\frac{V}{V_0} = 1$ and proceeds up in pressure as compression occurs. The difference between the thermodynamic pressure and the Rayleigh pressure at a given volume is equal to the viscous pressure, i.e., the last term on the right hand side of Eq. (27). Once initial compression has occurred, the chemical reaction occurs and the

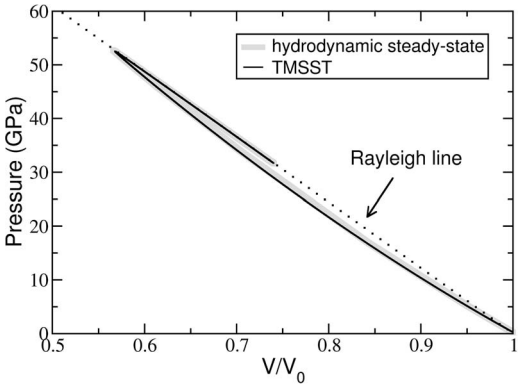

FIG. 4. Comparison of the thermodynamic pressure-volume space trajectory of the steady-state wave of direct hydrodynamic simulations to the TMSST technique. The Rayleigh line is shown by the dotted line. The simulation begins at $\frac{V}{V_0} = 1$ and proceeds up in pressure as compression occurs. Once initial compression has occurred, the chemical reaction occurs and the trajectory proceeds down the Rayleigh line. Since the chemical reaction results in volume changes slow enough for viscous effects to be negligible, the thermodynamic pressure is equal to the Rayleigh pressure during the chemical reaction portion of the shock.

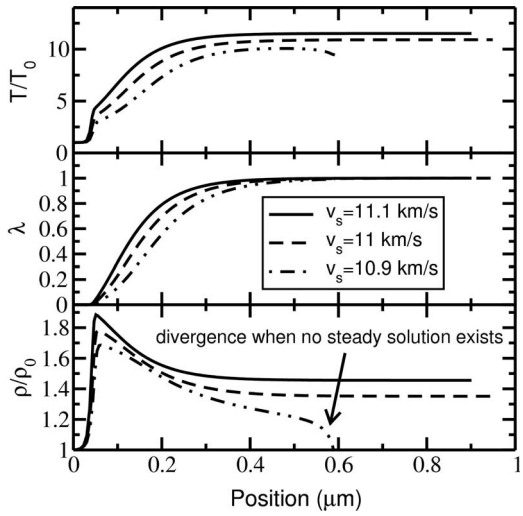

FIG. 5. Simulations at three different shock speeds using the TMSST in a model condensed phase explosive. Shocks at speeds 11.1 and 11.0 km/s represent overdriven detonation conditions as in the ACD path in Fig. 1. Shock speed 10.9 km/s is represented by path AB in Fig. 1 and is not a valid steady solution. In this case, the TMSST volume diverges when the shock wave mechanical stability conditions are no longer met, indicating there are no steady solutions for that shock speed. In this fashion the shock speed that takes the material to the sonic state (Rayleigh line AEF in Fig. 1) can be determined by bracketing with no prior knowledge of the equations of state or chemical reactions present.

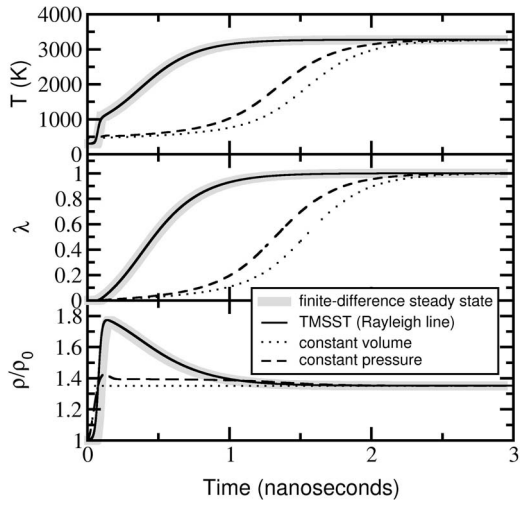

FIG. 6. Comparison of the time dependence of the thermodynamic trajectory of a material element flowing through a steady state wave in hydrodynamic simulations to various types of shock thermostatting techniques. The TMSST of this work is unique in that the intermediate states between the shock front and final state of the shock are correctly captured leading to a wave profile in agreement with hydrodynamic direct simulations. The model condensed phase explosive equation of state of Fig. 3 is utilized in these simulations.

trajectory proceeds down the Rayleigh line. Since the chemical reaction results in volume changes slow enough for viscous effects to be negligible, the thermodynamic pressure is equal to the Rayleigh pressure during the chemical reaction portion of the shock.

Similar to the ideal gas case, we find that the TMSST can be used to compute detonation wave profiles for physically reasonable large activation energies (e.g., $\epsilon_a = 50 k_B T_0$) as easily as for smaller activation energies. However, we find that increasing the activation energy beyond about $\epsilon_a = 9 k_B T_0$ with fixed $\tilde{q}$ can result in unsteady wave propagation in the hydrodynamic direct simulations. While the TMSST computes steady solutions for systems with large activation energies, it provides no information about the stability of these solutions to profile perturbations.

Figure 5 illustrates how the Chapman-Jouguet or sonic state (point F in Fig. 1) can be determined by performing simulations at multiple shock speeds. Figure 5 shows simulations at three different shock speeds using the TMSST with the model condensed phase explosive. Shocks at speeds 11.1 and 11.0 km/s represent overdriven detonation conditions as in the ACD path in Fig. 1. Shock speed 10.9 km/s is represented by path AB in Fig. 1 and is not a valid steady solution after the reaction parameter λ has increased beyond some critical value. In this case, the TMSST volume diverges when the shock-wave mechanical stability conditions are no longer met, indicating there are no steady solutions for that shock speed. In this fashion the shock speed that takes the material to the sonic state (Rayleigh line AEF in Fig. 1) can be determined by bracketing with no prior knowledge of the equations of state or chemical reactions present. In the case of Fig. 5, the shock speed that takes the system to the Chapman-Jouguet state is between 10.9 and 11 km/s.

IV. COMPARISON TO OTHER STYLES OF HUGONIOT-BASED CONSTRAINTS

A number of other styles of thermodynamic constraint schemes have been proposed for the molecular dynamics simulation of shock waves. In addition to a Hugoniot energy constraint or restraint on temperature, these schemes additionally constrain or restrain the system to constant volume [5], constant stress [7], or constant particle speed [6] rather than the Rayleigh line restraint utilized in this work. Figure 6 shows a comparison between several styles of thermodynamic constraining schemes for the model condensed phase explosive of Fig. 3. The schemes utilized here for constant volume and constant pressure are not identical to those of Refs. [5,7]. The constant volume curve was generated by solving the equation

$$\tilde{c}_v \dot{T} = \nu \left(\tilde{e} - \tilde{e}_0 - \frac{1}{2}(p + p_0)(\tilde{v}_0 - \tilde{v}) \right) \tag{28}$$

in conjunction with Eq. (21) for $\dot{\lambda}$. Here, $\tilde{v}$ is chosen to be the final volume of the shock wave. The constant pressure restraint curve in Fig. 6 was generated using Eq. (28) for the temperature evolution Eq. (21) for λ evolution, and the following equation for volume evolution:

$$\ddot{\tilde{v}} = \frac{1}{Q}(p - p_{\text{constraint}}) - \gamma\dot{\tilde{v}}, \tag{29}$$

where $p_{\text{constraint}}$ is the target pressure, taken to be the pressure of the final thermodynamic state of the shock. The parameters ν, Q, and γ were chosen to damp fluctuations in the thermodynamic state within about 100 ps. After this time, the thermodynamic trajectories are independent of these empirical parameters since the chemical reaction changes the thermodynamic state on a slower timescale.

Figure 6 shows that constant volume and constant stress approaches to thermostatting eventually achieve the correct final state of the shock, but take a thermodynamic trajectory to the final state that is different from the steady state wave of hydrodynamic simulations. The Rayleigh restraint utilized in the TMSST presented in this work captures the intermediate thermodynamic states in addition to the final thermodynamic state as well as the correct time dependence of the intermediate thermodynamic states. For a general equation of state with unknown reactions and phase transitions, the kinetics and even the final state of the shock can be determined by the thermodynamic pathway followed by the shocked material. We believe the TMSST and MSST are well suited to the study of such systems since they constrain the material element to the thermodynamic states found in the shock wave.

V. DISCUSSION AND CONCLUSION

In this work, we have considered equations of state with reaction rates that depend only on the temperature. In general, reaction rates can depend on other variables including strain rates and spatial gradients which can be quite large in shock waves. Some molecular dynamics simulations of shock waves show that very large spatial gradients in strain across a few atomic spacings can exist at the shock front (see, for example, Refs. [17,18]). In the TMMST and MSST, spatial strain gradients and spatial gradients in other thermodynamic quantities are neglected. As discussed in Ref. [8], it is therefore necessary to make the assumption that the material state and kinetics are not functions of spatial strain and thermodynamic gradients. The latter assumption is likely to be very good in liquids and molecular systems with little shear strength. Most energetic materials fall into this category. This assumption can potentially break down at sharp shock fronts in materials with long range correlation lengths. The latter type of system has not been addressed in this work.

In this work, we derived and analyzed a thermodynamic limit of a multiscale molecular dynamics based scheme that we have developed previously for simulating shock waves. We utilized a thermodynamic limit to validate and characterize the performance of the technique for several simple cases. Using analytical model equations of state for chemical reactions and kinetics in a gas and a condensed phase explosive, we showed that detonation wave profiles computed using the computational scheme are in good agreement with the steady state wave profiles of hydrodynamic direct numerical simulations. We also characterized the stability of the technique when applied to detonation waves and described a technique for determining the detonation shock speed for a chemically reactive equation of state about which nothing is known *a priori*.

ACKNOWLEDGMENT

This work was performed under the auspices of the U.S. Department of Energy by the University of California, LLNL under Contract No. W-7405-Eng-48.

[1] J. D. Kress, S. R. Bickham, L. A. Collins, B. L. Holian, and S. Goedecker, Phys. Rev. Lett. **83**, 3896 (1999).
[2] M. D. Knudson and Y. M. Gupta, Phys. Rev. Lett. **81**, 2938 (1998).
[3] C. S. Yoo, W. J. Nellis, M. L. Sattler, and R. G. Musket, Appl. Phys. Lett. **61**, 273 (1992).
[4] E. M. Bringa, J. U. Cazamias, P. Erhart, J. Stolken, N. Tanushev, B. D. Wirth, R. E. Rudd, and M. J. Caturla, J. Appl. Phys. **96**, 3793 (2004).
[5] J. B. Maillet, M. Mareschal, L. Soulard, R. Ravelo, P. S. Lomdahl, T. C. Germann, and B. L. Holian, Phys. Rev. E **63**, 016121 (2000).
[6] E. J. Reed, J. D. Joannopoulos, and L. E. Fried, in *Shock Compression of Condensed Matter 2001* (American Institute of Physics, New York, 2001), p. 343.
[7] R. Ravelo, B. L. Holian, T. C. Germann, and P. S. Lomdahl, Phys. Rev. B **70**, 014103 (2004).
[8] E. J. Reed, L. E. Fried, and J. D. Joannopoulos, Phys. Rev. Lett. **90**, 235503 (2003).
[9] E. J. Reed, L. E. Fried, M. R. Manaa, and J. D. Joannopoulos, in *Chemistry at Extreme Conditions*, edited by M. R. Manaa (Elsevier, New York, 2005), p. 297.
[10] H. C. Andersen, J. Chem. Phys. **72**, 2384 (1980).
[11] M. P. Allen and D. J. Tildesley, *Computer Simulation of Liquids* (Oxford University Press, New York, 1989).
[12] Y. B. Zel'dovich and Y. P. Raizer, *Physics of Shock Waves and High-temperature Hydrodynamic Phenomena* (Academic Press, New York, 1967).
[13] W. Fickett and W. Davis, *Detonation* (University of California Press, Berkeley, CA, 1979).
[14] L. Verlet, Phys. Rev. **159**, 98 (1967).
[15] L. Verlet, Phys. Rev. **165**, 201 (1967).
[16] G. E. Duvall, in *Proceedings of the International School of Physics, Physics of High Energy Density* (Academic Press, New York, 1971), p. 7.
[17] D. W. Brenner, D. H. Robertson, M. L. Elert, and C. T. White, Phys. Rev. Lett. **70**, 2174 (1993).
[18] V. V. Zhakhovskiĭ, S. V. Zybin, K. Nishihara, and S. I. Anisimov, Phys. Rev. Lett. **83**, 1175 (1999).

[19] W. Henshaw, Lawrence Livermore National Laboratory Research Report No. UCRL-MA-134288 (unpublished).
[20] W. D. Henshaw and D. W. Schwendeman, J. Chem. Phys. **191**, 420 (2003).
[21] R. Leveque, *Finite Volume Methods for Hyperbolic Problems* (Cambridge University Press, Cambridge, England, 2004).
[22] D. N. Williams, L. Bauwens, and E. S. Oran, Shock Waves **6**, 93 (1996).
[23] D. Lemons and C. Lund, Am. J. Phys. **67**, 1105 (1999).